

# Re-Nerfing: Improving Novel View Synthesis through Novel View Synthesis

Felix Tristram<sup>\*,1</sup> Stefano Gasperini<sup>\*,1,2</sup> Nassir Navab<sup>1</sup> Federico Tombari<sup>1,3</sup>  
<sup>1</sup> Technical University Munich <sup>2</sup> VisualAIs <sup>3</sup> Google

## Abstract

Recent neural rendering and reconstruction techniques, such as NeRFs or Gaussian Splatting, have shown remarkable novel view synthesis capabilities but require hundreds of images of the scene from diverse viewpoints to render high-quality novel views. With fewer images available, these methods start to fail since they can no longer correctly triangulate the underlying 3D geometry and converge to a non-optimal solution. These failures can manifest as floaters or blurry renderings in sparsely observed areas of the scene. In this paper, we propose *Re-Nerfing*, a simple and general add-on approach that leverages novel view synthesis itself to tackle this problem. Using an already trained NVS method, we render novel views between existing ones and augment the training data to optimize a second model. This introduces additional multi-view constraints and allows the second model to converge to a better solution. With *Re-Nerfing* we achieve significant improvements upon multiple pipelines based on NeRF and Gaussian-Splatting in sparse view settings of the mip-NeRF 360 and LLFF datasets. Notably, *Re-Nerfing* does not require prior knowledge or extra supervision signals, making it a flexible and practical add-on.

## 1. Introduction

Novel view synthesis (NVS) methods based on Neural Radiance Field (NeRF) [37] and 3D Gaussian Splatting (3DGS) [28] have recently revolutionized 3D scene representation and rendering, enabling unprecedented quality in synthesizing novel views from a set of images. These techniques have been applied across various tasks, simplifying content creation, rendering, and reconstruction workflows.

Despite its remarkable success, NeRF [37] has several limitations, such as slow training [38], failures when noisy or no camera poses are available [4, 33], and computationally intense rendering mostly incompatible with mobile applications [12]. Many works have been proposed to address

\* The authors contributed equally.

Contact author: Felix Tristram ([felix.tristram@tum.de](mailto:felix.tristram@tum.de)).

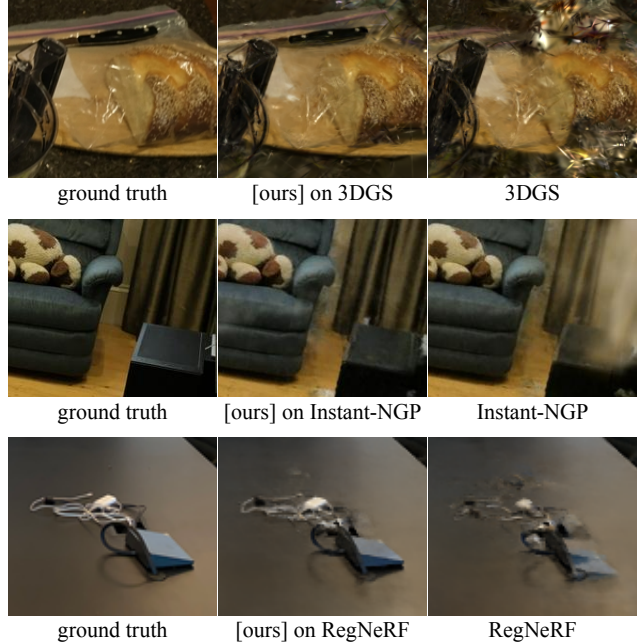


Figure 1. Examples of synthesized views by 3DGS [28], Instant-NGP [38], RegNeRF [40], with and without the proposed Re-Nerfing. Our approach improves NVS by improving the optimization, reaching better global solutions thanks to the addition of novel views synthesized by the baseline model to the training data. Image crops show test views from the mip-NeRF 360 [3] dataset for 3DGS, iNGP trained on 30 views and from the LLFF [36] dataset for RegNeRF trained on 3 views.

these issues, such as 3DGS [28] changing representation to shorten training times and simplifying inference. However, collecting enough high-quality images with sufficient overlap to ensure successful model convergence remains a challenging task. Towards this end, researchers have explored the application of NVS in sparse view settings, with only a handful of images available [40, 58, 66].

Complex geometries and large-scale environments often lead to artifacts due to the inability to correctly triangulate the scenes’ 3D structure [2, 15, 49]. This is particularly severe in sparse settings, where the limited views lead to hallucinations, e.g. floaters in free space due to the ambiguity of shape and radiance [15, 34, 58]. To mitigate these

issues, depth and structural priors have been introduced to the optimization to leverage additional geometric information [15, 49, 58]. However, reliable dense depth estimates are also hard to obtain, and using wrongly estimated depth can further hurt performance [15].

In this work, we mitigate these open issues with a simple and effective add-on solution exploiting the inherent novel view synthesis capability of NVS methods. We achieve this with Re-Nerfing, a multi-stage, general pipeline that introduces structural constraints from synthetic views generated by a previously trained model on the same scene. As shown in Figure 1, thanks to its ability to improve the view coverage while preserving quality discarding uncertain regions, Re-Nerfing significantly improves the synthesis of new views. The main contributions of this paper can be summarized as follows:

- With Re-Nerfing, we show how NeRF’s and Gaussian Splatting’s novel view synthesis is beneficial to enhance their own rendering quality.
- We propose a simple and effective iterative augmentation technique to enhance any NVS outputs by training a new NVS model with the addition of synthesized views selected to improve the scene coverage and masked to discard uncertain areas.
- We show the wide applicability of Re-Nerfing upon various NVS pipelines [28, 38, 40, 59] and datasets [3, 36].

## 2. Related Work

Given a dense set of images, traditional interpolation techniques based on light field sampling can synthesize photorealistic novel views [31]. In relatively sparser settings, neural networks have been used for view synthesis by exploiting the correlation of the visual appearance of an instance across different views [19, 64]. More recently, 3DGS [28] has shown great promise in view synthesis tasks by optimizing the scene as 3D Gaussians with spherical harmonics.

Neural implicit representations have emerged as a shift from traditional explicit representations like point clouds, meshes, and voxels [46, 65], by encoding 3D shapes implicitly in the weights of a neural network. The pioneering works of Occupancy Networks [35] and DeepSDF [42] initiated this line of work by encoding complex shapes in a continuous function space through a network. Unlike traditional representations, here, no space discretization is needed, enabling finer details [53].

**NeRF** Mildenhall et al. [37] introduced NeRF by combining neural implicit representations with differentiable rendering, encoding both volumetric properties and view-dependent appearance and leading to high-quality novel views. NeRF has catalyzed a myriad of works tackling various aspects of its limitations and further improving NVS [61]. Among these, Instant-NGP [38], FastNeRF [22] and others [8, 20, 54] enable significantly faster training

speeds, BARF [33], SPARF [58] and Nope-NeRF [4] cope with imperfect or absent camera poses, mip-NeRF 360 [3] deals with unbounded scenes and Nerfies [43] among others [7, 21, 44] deals with dynamic scenes. Additionally, the work of Rössle et al. [49] delivers more consistent geometry, CoNeRF [27] enables altering the output, Panoptic Neural Fields [29] incorporates scene understanding information, Block-NeRF [55] renders city-scale scenes, and Camp [45] optimizes the camera parameters. PyNeRF [59] combines the benefits of mip-NeRF [2] and grid-based models, such as Instant-NGP, to facilitate fast training and rendering of anti-aliased images.

**Sparse settings** Nevertheless, highly sparse settings are particularly challenging as the standard multi-view constraints are not sufficient [13, 58]. Strong geometric information is required to reconstruct the scene and enable satisfactory novel views synthesis. Towards this end, researchers have explored the support of additional data and external models to provide geometric supervision [49, 58] or semantic knowledge [47, 62]. Such techniques enable NVS even from a single image. SPARF [58], for example, relies on a pixel correspondence network to enforce a geometrically accurate solution. PixelNeRF [62] learns a prior from multiple scenes and conditions the novel views on the few inputs available. For Gaussian Splatting-based methods, multiple extensions have been proposed to deal with sparse view settings [17, 32, 41, 66]. However, all aforementioned methods depend on external models and large amounts of training data, which eliminates the advantage of NeRF and 3DGS of not requiring any training data other than that for the object or scene of interest.

**Geometric constraints** Enforcing geometric consistency plays a crucial role in NVS as it directly impacts the quality of the generated views [49]. DS-NeRF [15] supervises NeRF’s optimization with sparse depth obtained from COLMAP [51], thereby reducing overfitting and accelerating training. Rössle et al. [49] went a step further by feeding the sparse COLMAP point cloud to a depth completion network and constraining NeRF’s optimization according to the estimated depth and its associated uncertainty. Urban Radiance Fields [48] focuses on outdoor scenes where LiDAR data is available, which is used for losses that benefit surface estimation. FSGS [66] and related methods [32, 41] on the other hand rely on monocular depth prediction to acquire a good geometry initialisation and supervision signal. SPARF [58] exploits multi-view geometry constraints and pixel correspondences, minimizing the re-projection error using the depth rendered by the NeRF and the pose estimates, which are optimized jointly.

**Data augmentation for NVS** In general, data augmentation aims to increase the pool of training data with samples that are variations of the existing ones (e.g., image flip), ultimately regularizing the model. As for other computer

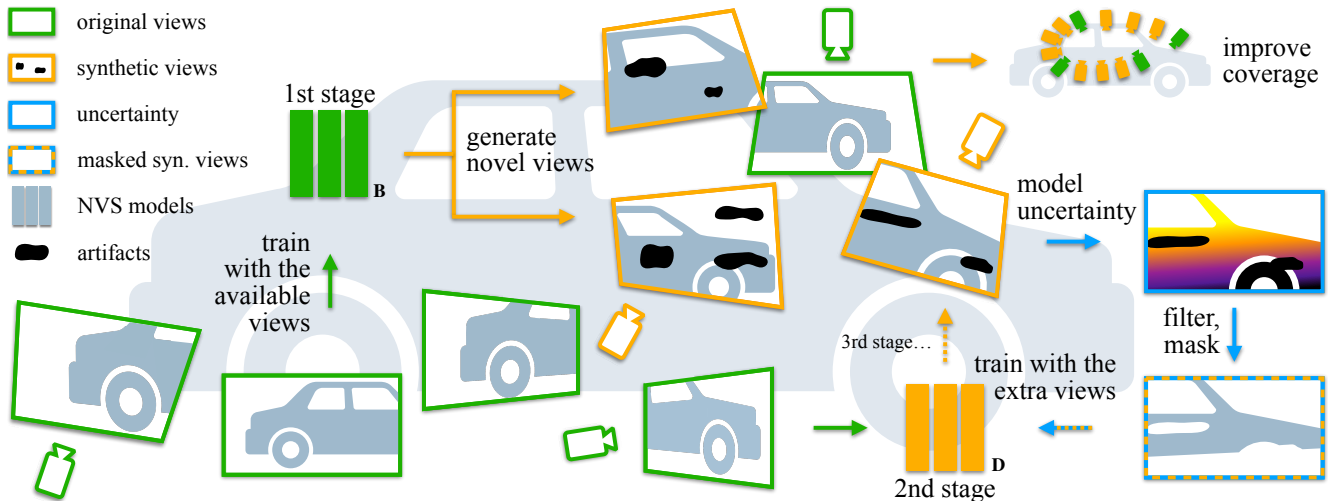


Figure 2. Re-Nerfing is a multi-stage framework. Compatible with any NVS pipeline, it operates by first training a model with the available views (green, 1st). This model is then used to generate novel views from camera poses to improve the scene coverage (orange). Then, we compute the model’s uncertainty on such novel views (blue) and discard the uncertain regions (orange-blue). Finally, we use these masked views and the original ones to train a second model (orange, 2nd). The process can be repeated iteratively by generating the novel views with the second model (3rd stage).

vision tasks and settings [24, 30, 39], data augmentation techniques have also been proposed for NVS. In this domain, PANeRF [1], GeoAug [9], and VM-NeRF [5] generate new views by warping existing ones via homography [1] or exploiting the NeRF’s depth estimates [5, 9]. In contrast, Aug-NeRF [11] trains more robust NeRFs with worst-case perturbations of the input coordinates, the intermediate features, and the pre-rendering outputs.

**Distillation and semi-supervised learning** Knowledge distillation involves transferring knowledge from a large, complex model (teacher) to a smaller, more efficient one (student) [26]. This paradigm has been widely adopted and extended to semi-supervised learning, from segmentation [10] to depth estimation [23]. Naive-student [10] predicts pseudo-labels for a set of unlabeled data and later trains a new model using the original data and the newly pseudo-labeled samples. Tosi et al. [57] achieved remarkable depth estimates by training a stereo depth model using data synthesized by NeRF. NeRFmentation [18] trains a NeRF model and uses it to generate augmented data for a monocular depth estimator.

In this work, we enhance NVS in sparser settings by exploiting the NVS method’s inherent view synthesis capabilities. Unlike existing approaches [48, 49, 58, 62], we do so in a data augmentation manner by using only the available views without extra data or additional models. We achieve this by training a baseline NVS method on the available data and using it to generate novel views that we add to the training data of a subsequent NVS model. Specifically, we sample such views to improve the scene coverage while preserving the images’ quality by masking out uncertain re-

gions. In contrast to Tosi et al. [57] and Feldmann et al. [18], who trained a depth estimator with NeRF data, we train an NVS model with other NVS data. Then, unlike other augmentation methods [1, 5, 9], our newly introduced views are fully synthesized from an NVS model.

### 3. Method

As shown in Figure 2, our proposed Re-Nerfing operates in a multi-stage fashion. First, a baseline method is trained with the available views (Section 3.1), then it is used to generate novel views to improve the scene coverage (Section 3.2), and lastly, a new model is trained on the original and the synthetic views (Section 3.3), discarding uncertain regions of the rendered views to improve the signal’s quality. Re-Nerfing is a general framework that is compatible with any pipeline for NVS. Furthermore, Re-Nerfing follows an iterative process, so further rounds can be executed using the model trained at the previous iteration as a baseline for the next one.

#### 3.1. NeRF and 3DGS Optimization

To better understand the shortcomings of NeRF [37] and 3DGS [28] optimizations in a sparser setting, we review how they optimize their scene representation and render images from it. Both methods are optimized through photometric consistency, where the color of each ray or pixel is compared to the ground truth color with an L2 loss or a mixture of L1 and SSIM losses [28]. This color is obtained through volumetric rendering via the following equations, where density  $\sigma$ , Transmittance  $T$ , and color  $c$  are taken

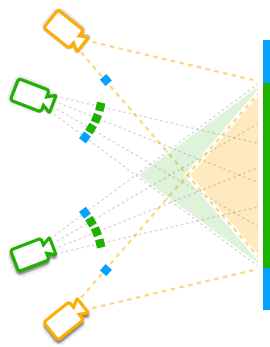
along a ray or z-value at intervals  $\delta_i$ :

$$C = \sum_i^N T_i \alpha_i \mathbf{c}_i, \quad (1)$$

where

$$\alpha_i = (1 - \exp(-o_i \delta_i)) \quad \text{and} \quad T_i = \prod_{j=1}^{i-1} (1 - \alpha_j). \quad (2)$$

This formulation holds for both NeRF-based architectures and neural point-based rendering approaches, such as 3DGS [28], where the image formation process is the same but images are rendered through ray-tracing or rasterization.



To represent the geometry of the given scene only the density  $o_i$  at sampling or point locations can be optimized. If very few images of the scene are given, this density can no longer be correctly triangulated since there are not enough multi-view constraints and too much ambiguity in the color supervision. This can be seen in the simplified exam-

ple in the inset, where the green cameras represent the original ones and the shaded green region represents valid solutions where density could be distributed. The overall optimization process would converge to one of the many valid solutions within the green region, i.e., a local minimum, leading to dissatisfying geometry reconstruction and poor NVS.

### 3.2. Augmenting via Synthesized Views

As introduced above, sparse view reconstruction is a highly under-constrained problem. In scenarios without enough views, e.g., due to crowd-sourced or previously captured images, NVS is particularly difficult. Various methods tackled this with prior knowledge [15, 58] or regularization [40]. Instead, we propose to leverage the inherent reconstruction and rendering capabilities of NVS methods to render novel views and utilize these rendered images as *additional training data* in subsequent optimizations (Section 3.3), thereby introducing additional multi-view constraints *without* prior knowledge or external models.

We motivate this approach with the simplified example in the inset figure (Section 3.1, where the orange cameras represent novel views rendered after the first optimization, and the green cameras are the originally available views. By introducing these additional views, possible solutions reduce from the green-shaded region to the orange-shaded region, making triangulation of the scene’s geometry/density

easier. We then re-start the optimization from scratch (Section 3.3). Thanks to the additional viewpoints present in the training data, we can avoid some of the previously present local minima and converge to a better global solution for the given NVS method.

**View coverage** We seek to improve the view coverage of the captured scene or object through our augmentations. This is particularly relevant in sparser settings. Toward this end, we generate multiple novel views from camera poses interpolated across existing neighboring views. We define the hyperparameters  $N$  and  $\Omega$ , being the augmentation factor and the set of  $N - 1$  interpolation factors  $\beta_j$ , respectively. Specifically, for the simple case of equally spaced novel views:

$$\Omega = \left\{ \beta_j \mid \beta_j = \frac{j}{N}, j = 1, 2, \dots, N - 1 \right\} \quad (3)$$

However, equally spaced synthesized views are not ideal as the quality would degrade around  $\beta = 0.5$ . This is particularly relevant in sparser settings where the larger camera displacement between existing poses would lead to worse synthetic views. This is illustrated in the Supplementary Material.

Considering the existing camera poses  $\mathbf{P}_i$  and  $\mathbf{P}_{i+1}$  with  $\mathbf{P} = [\mathbf{p}, \mathbf{q}]$ , such that  $\mathbf{p}$  is the position vector in 3D space and  $\mathbf{q}$  is the quaternion representation of the rotation,

$$\bar{\mathbf{p}}_{i,j} = (1 - \beta_j)\mathbf{p}_i + \beta_j\mathbf{p}_{i+1} \quad (4)$$

is the interpolation of the position component given an interpolation factor  $\beta_j$ . For the rotation, we compute the interpolated  $\bar{\mathbf{q}}_{i,j}$  from the original pose quaternions  $\mathbf{q}_i$  and  $\mathbf{q}_{i+1}$  using SLERP [52] as follows:

$$\bar{\mathbf{q}}_{i,j} = \frac{\sin((1 - \beta_j)\theta)}{\sin(\theta)}\mathbf{q}_i + \frac{\sin(\beta_j\theta)}{\sin(\theta)}\mathbf{q}_{i+1} \quad (5)$$

Instead of interpolating across existing views, other strategies could generate novel views around a half dome centered at the scene or object center, or following a specific pattern. However, in real-world scenes, such techniques may raise issues with occlusions, as the sampled poses might collide with parts of the scene (e.g., wall) or end up inside an object. Interpolating is more conservative and does not require extra information about the scene, such as the scene occupancy, to avoid collisions and unrealistic viewpoints. Nevertheless, multiple pose sampling strategies could be combined to further enhance the view synthesis.

The formulation above is based on two consecutive poses  $\mathbf{P}_i$  and  $\mathbf{P}_{i+1}$ . In settings where sequential information is not available, a sequence can be simulated by considering consecutive poses from neighboring positions in 3D space [14]. This can be achieved with a nearest neighbor on the vectors  $\mathbf{p}$  using the Euclidean distance or the angular distance between the quaternions  $\mathbf{q}$ .

**Image Quality** Our proposed method has to balance the synthesized image quality with achieving as wide a baseline as possible with regard to the original views. This is because novel views close to the training views will be of higher quality and exhibit less artifacts compared to ones which are further away but add less multi-view constraints. In practice we achieve this trade-off through generating many interpolated views between the original training views  $\mathbf{P}_i$  and  $\mathbf{P}_{i+1}$  and achieve a good balance between both factors. We illustrate the trade-off in the supplementary material.

### 3.3. Re-Nerfing: Re-Training NeRF or 3DGS

After training the first model  $\mathbf{B}$  and using it to generate novel views (Section 3.2), we train another NVS method  $\mathbf{D}$  from scratch with the addition of the synthesized views. To improve the signal’s quality, we mask out uncertain regions of the generated views with Bayes’ Rays [25], where possible.

**Uncertainty masks** We seek to add a high-quality training signal to the new model  $\mathbf{D}$  by means of the synthesized views. Since the quality of such views is not on par with the originals, they may display artifacts that can impact the renderings. Therefore, we want to remove such artifacts and improve the training signal. One way of estimating the reconstruction uncertainty is to use Bayes’ Rays [25], which can be used to mask out more uncertain regions from our synthesized images. Bayes’ Rays [25] outputs a volumetric uncertainty field for every input coordinate  $\mathbf{x}$ :

$$U(\mathbf{x}) = \text{Trilinear}(\mathbf{x}, \sigma), \quad \text{where } \sigma = \|\sigma\|_2 \quad (6)$$

Here  $\sigma = (\sigma_x, \sigma_y, \sigma_z)$  represents the diagonal entries of the variance  $\Sigma$  of the deformation field, which intuitively encodes how much one can permute the underlying NeRF geometry without affecting reconstruction quality.  $\Sigma$  is approximated via the diagonal entries of the Hessian  $\mathbf{H}(\theta)$ , which is approximated for all rays  $\mathbf{r}$  of a sampling pool  $R$  with respect to the parameters  $\theta$  of the deformation field as:

$$\mathbf{H}(\theta) \approx \frac{2}{R} \sum_{\mathbf{r}} \mathbf{J}_{\theta}(\mathbf{r})^T \mathbf{J}_{\theta}(\mathbf{r}) + 2\lambda \mathbf{I} \quad (7)$$

$$\Sigma \approx \text{diag}(\mathbf{H}(\theta))^{-1} \quad (8)$$

For the full derivation of this formulation we refer the reader to the original publication of Bayes’ Rays [25].

The uncertainty obtained at each sampling location  $\mathbf{x}$  can then be rendered via volumetric rendering. Specifically, for each ray  $\mathbf{r}$  of a novel pose  $\mathbf{P}$  with ray samples  $\mathbf{x}$ , we synthesize the color  $C_{\mathbf{B}}(\mathbf{r})$  and render the corresponding uncertainty  $U(\mathbf{r}(\mathbf{x}))$ . Then, we create pixel-masks where rays with  $U(\mathbf{r}(\mathbf{x}))$  higher than a threshold  $\mu$  are masked out. To optimize the second model  $\mathbf{D}$ , we use the generated views as part of the training images and query their masked rays during the course of optimization.

**Training Schedule** For both NeRF and 3DGS the scene geometry is reconstructed in the early optimization stages and later they are optimized for appearance. Since the synthesized views are not as good as real images, especially when generated at positions further away from the training views, they can become a sub-optimal signal when optimizing for appearance. Therefore, we sample from our synthesized images only in the early stages of the optimization, where they help disambiguating the scene geometry, and then remove them from the training as they start to become detrimental to the appearance optimization.

**Third and later stages** The proposed method uses a base model  $\mathbf{B}$  to augment the training data for a later model  $\mathbf{D}$ . This introduces a general paradigm that can be repeated iteratively until the gain saturates. Therefore, new augmented views can be synthesized with  $\mathbf{D}$  and masked to train a new model  $\mathbf{D}_2$ , and so on. As our synthesized data augmentation regularizes the later models  $\mathbf{D}_n$ , these are less prone to overfitting on the initial views, which would allow us to increase the model size and reach higher quality. However, this is out of the scope of this work, as we use identical architectures across the iterations.

## 4. Experiments and Results

Since having a more diverse set of views during the start of optimization benefits reconstruction, we observe faster convergence on the test views when using Re-Nerfing. Interestingly, not only does using Re-Nerfing improve convergence speed and test-view quality but it can also boost PSNR values on the training views, further reinforcing our intuition.

### 4.1. Experimental Setup

**Dataset and metrics** We test our method on the challenging 7 public scenes introduced with **mip-NeRF 360** [3], comprising both bounded indoor and large unbounded outdoor settings. Additionally, we experimented with the 8 scenes of the **LLFF** dataset [36], which includes smaller, bounded scenes. The former features a large amount of real images captured all around an object or scene, while the latter has fewer views of forward-facing scenes. So, the two assess complementary aspects. For sparsifying the mip-NeRF 360 dataset, we select the training views by sampling from all available images (including the test ones) while preserving as much coverage of the scene as possible. We then select the test views among those test views from the original set that were not selected as training images. Toward this end, we selected 30 training images (50 for *stump* and *bicycle* due to convergence issues of the baselines when using 30 views). The exact data splits will be made available. With LLFF, we experimented with the highly sparse setting with just 3 views available, following the evaluation paradigm of RegNeRF [40]. We evaluate the test views on the standard metrics and errors, i.e., PSNR, SSIM [60], and LPIPS [63].

Method	PSNR	SSIM	LPIPS
Instant-NGP [38]	20.76	0.659	0.301
+ Re-Nerfing [ours]	<b>21.35</b>	<b>0.680</b>	<b>0.273</b>
PyNeRF [59]	22.65	0.746	0.182
+ Re-Nerfing [ours]	<b>23.51</b>	<b>0.772</b>	<b>0.160</b>
3DGS [28]	20.49	0.600	0.259
+ Re-Nerfing [ours]	<b>21.30</b>	<b>0.627</b>	<b>0.235</b>

Table 1. Rendering performance on the mip-NeRF 360 [3] dataset in **sparse view settings** averaged over the scenes. The proposed Re-Nerfing is applied on the Instant-NGP [38], PyNeRF [59], and 3DGS [28] baselines, using the corresponding baseline to augment the views. Uncertainty estimates are unavailable for 3DGS.

**Prior Works and Baselines** We showcase the effectiveness of our method by applying it on diverse NVS methods, namely PyNeRF [59], Instant-NGP [38], RegNeRF [40], and 3DGS [28]. 3DGS uses an explicit representation, so there is no model uncertainty to estimate. RegNeRF, on the other hand, is implemented in JAX [6], for which no implementation of Bayes’ Rays [25] exists. Therefore, with 3DGS and RegNeRF, we show only the impact of our augmentations without uncertainty masks.

**Implementation Details** We train our method on an image resolution down-sampled by eight from the original image sizes for the available outdoor scenes and down-sampled by four for the indoor scenes of the mip-NeRF360 dataset, bringing both to a comparable image size. For the LLFF dataset we down-sample all images by eight, following RegNeRF [40]. All models are trained using Nerfstudio [56], except for RegNeRF where we use the original implementation in JAX [6]. For PyNeRF [59], Gaussian Splatting [28] and Instant-NGP [38], we used their implementation available in Nerfstudio. We trained all Nerfstudio models for 30k iterations from scratch with a batch size of 8192 rays for PyNeRF and 1024 rays for Instant-NGP and inherited all other losses and hyperparameters of the baseline methods. For RegNeRF we followed their training paradigm and hyperparameters. The influence of the synthesized views on the optimization is removed after 8k iterations for PyNeRF and Gaussian-Splatting, after 5K iterations for RegNeRF and after 200 iterations for Instant-NGP. We train all models on a 24GB NVIDIA RTX 3090 or 4090 GPU.

## 4.2. Quantitative Results

In Table 1, we report the results on the mip-NeRF 360 dataset [3] applying the proposed Re-Nerfing on Instant-NGP [38], PyNeRF [59], and 3D Gaussian Splatting [28] in sparse view settings. In Table 2, we report the results on the LLFF dataset [36] applying Re-Nerfing on RegNeRF [40] in highly-sparse 3 view settings.

3 Views	PSNR	SSIM	LPIPS
baseline: mip-NeRF [2]	14.62	0.351	0.495
+ RegNeRF [40]	19.08	0.685	0.148
+ Re-Nerfing, 1 round [ours]	19.35	0.713	0.133
+ extra round, 2nd [ours]	<u>19.47</u>	<u>0.724</u>	<b>0.126</b>
+ extra round, 3rd [ours]	<b>19.52</b>	<b>0.725</b>	<u>0.127</u>

Table 2. Highly sparse settings with only **3 views** on the LLFF dataset [36]. We apply ours on top of RegNeRF [40]. Then, we iteratively apply ours via the extra rounds. The results are averaged over all LLFF scenes.

**Re-Nerfing as flexible add-on** The proposed method brings notable improvements across various settings, increasing PSNR by 0.86 dB over PyNeRF, 0.81 dB over 3DGS, 0.64 dB over Instant-NGP, and 0.27 dB over RegNeRF already with a single iteration, while improving SSIM and LPIPS as well. Despite their synthesized nature, adding more training views mitigates overfitting and acts as a regularizer. In Table 2, in particular, we combine Re-Nerfing with the regularization of RegNeRF, showing how Re-Nerfing can adapt to any NVS method. This is because it is an add-on and not an alternative to them. Overall, the efficacy of our method on both implicit (NeRF-based) and explicit (3DGS) scene representations is particularly notable as it is achieved without using extra data, additional models, or supervision, but only with already available information.

**Re-Nerfing as an iterative method** In Tables 2 and 3, we show the impact of our method when applying it iteratively. As described in Section 3.3, Re-Nerfing uses renderings from a first model **B** to augment the training data of a second model **D**. To further improve the output quality, the process can be repeated iteratively, by using **D** to render the augmented views. We show this in the tables, where, at each iteration, the quality improves across the board for the various pipelines and settings. This confirms that NVS helps the task of NVS. While the improvement varies from scene to scene, we notice that the performance saturates beyond 3-5 rounds. Overall, the proposed Re-Nerfing leads to a substantial boost of **+3.45 PSNR over 3DGS [28]**, without using any extra data or external models, other than what is already available to the standard 3DGS.

**Why it works** As described in Section 3.1, NeRF’s and 3DGS’ optimization is similar to SfM approaches, as matching pixel features are triangulated in 3D. Especially in sparse settings, this is highly under-constrained with many degenerate solutions. This can lead to local minima, which fit well with the training views but not the test views due to the inconsistent geometry. With Re-Nerfing, we build upon this (potentially sub-optimal) initial optimization and render synthetic views as extra constraints for later rounds. It is widely known that more viewpoints help NVS. This same concept drives Re-Nerfing, too, albeit with synthe-

Method	3DGS [28]			PyNeRF [59]		
	PSNR	SSIM	LPIPS	PSNR	SSIM	LPIPS
baseline	19.31	0.609	0.296	17.57	0.643	0.325
+ [ours]: 1	21.08	0.686	0.241	18.09	0.676	0.299
+ [ours]: 2	21.89	0.720	0.214	18.36	0.693	0.285
+ [ours]: 3	22.47	0.748	0.191	18.41	0.699	0.281
+ [ours]: 4	<u>22.63</u>	<u>0.756</u>	<u>0.184</u>	<u>18.47</u>	<u>0.704</u>	<u>0.275</u>
+ [ours]: 5	<b>22.76</b>	<b>0.761</b>	<b>0.178</b>	<b>18.64</b>	<b>0.708</b>	<b>0.272</b>

Table 3. Rendering performance on the mip-NeRF 360 [3] *counter* scene in the 30-view setting. Re-Nerfing is applied iteratively across multiple rounds, from 1 to 5.

sized views. Thanks to these extra constraints, some degenerate solutions are removed and the optimization converges to a better 3D structure. This can be seen in the supplementary video, with smoother rendered depth maps. Through an ablation study on 3DGS [28], Table 5 shows the importance of: early optimization stages for the scene geometry and the impact of the pseudo views (syn.views) on that, removing the pseudo views as the scene geometry converges to not learn wrong details from them, and resetting the training at each of the Re-Nerfing rounds. Specifically, adding the synthetic views without resetting the optimization (3rd row) does not bring any benefits and worsens LPIPS. Resetting and keeping the rendered views until the end (4th row) improves, but removing them leads to better details (last row, ours). On the contrary, adding the views after the scene geometry has already been captured (5th row) leads to mixed results compared to the baselines. While Re-Nerfing increases the training iterations, e.g., by 2x in the table, simply doubling the iterations performs worse (2nd row). All together, Re-Nerfing leads to a better global solution without adding extra info over the baseline. This is similar

Method	PSNR	SSIM	LPIPS
1x: PyNeRF [59], baseline	22.42	0.632	0.218
1.08x: 4 random syn.views	22.58	0.653	0.205
1.08x: 4 test syn.views	<b>22.64</b>	<b>0.663</b>	<b>0.196</b>
2x: .50	23.35	0.669	0.190
3x: .33-.66	23.40	0.666	0.191
3x: .20-.80	23.61	0.670	0.189
3x: .10-.90	23.47	0.670	0.191
4x: .25-.50-.75	23.51	0.667	0.192
5x: .2-.4-.6-.8	23.63	0.668	0.189
7x: 5x + .1-.9 [selected]	<b>23.73</b>	<b>0.672</b>	<b>0.184</b>
11x: 7x + .05-.3-.5-.7-.95	23.48	0.669	0.189

Table 4. View selection strategies on the *stump* 50-view setting of the mip-NeRF 360 [3] dataset. Models based on PyNeRF [59]. Our augmentation factors  $N$  from 2 to 11 are evaluated.

sparse views	PSNR	SSIM	LPIPS
baseline: 3DGS [28], 30k iter.	19.31	0.609	0.296
2x longer training (60k iter.)	19.68	0.633	0.274
no reset, add syn.views at 30k	19.67	0.631	0.333
reset, add and keep syn.views	20.15	0.654	0.291
reset, add syn.views at 15k	19.79	0.637	0.325
reset, remove syn.views at 8k	<b>21.08</b>	<b>0.686</b>	<b>0.241</b>

Table 5. Ablation study. 30-view setting, *counter* scene of the mip-NeRF 360 dataset [3] with 3DGS [28]. The last row represents the proposed method.

to other iterative frameworks from other domains [10, 23], where resetting the optimization at each round leads to better solutions.

**Trade-offs with pseudo-views poses** In Table 4, we evaluate different poses for the novel view selection on PyNeRF [59], exploring different interpolations across pairs of the original views. Remarkably, all augmentations are beneficial, improving PSNR by 0.9-1.3 dB. The results show the trade-offs further described in the supplementary material: the furthest from the original views (e.g., .33-.66 is further than 0.20-0.80), the lower the quality of the novel views, and the smaller the performance improvement. However, the opposite trade-off occurs, too: the closer to the initial images, the less amount of new information to gain for the multi-view optimization. Therefore, it is better to sample more pseudo-views closer to the original ones while still including further viewpoints for extra information, as for 7x.

**Impact of the augmentation factor** In Table 4, we also explore different augmentation factors  $N$ . Higher factors are more beneficial despite the introduction of more sub-optimal, synthesized views. Doubling the views (2x) brings the largest relative gain with +0.9 dB PSNR. The performance further improves as the factor is increased. However, at high  $N$  factors (e.g., 11x), benefits reduce as the influence of the many synthetic views overcomes the few original images, with 7x striking a good balance.

**Optimizing for specific views** In Table 4, we show how we can optimize for specific views, by augmenting with 4 test views synthesized by the baseline. We compare this with augmenting with 4 randomly interpolated views and evaluate on the viewpoint of the 4 test views. While adding random views helps, specifically synthesizing the viewpoints of interest (e.g., the test views) shows higher margins on all metrics. In practice, Re-Nerfing allows to improve on viewpoints of interest, which can be beneficial when the available views lead to a sub-optimal quality in specific areas. In such settings, Re-Nerfing can densify the views around such areas and ultimately improve the outputs.



Figure 3. Qualitative results on cropped images from the test set of the mip-NeRF 360 and LLFF datasets. 3DGS [28] and Instant-NGP [38] were trained on the mip-NeRF 360 dataset in a 30 view setting, while RegNeRF [40] was trained on LLFF with only 3 views. Qualitative results of PyNeRF [59] can be found in the supplementary material.

### 4.3. Qualitative Results

Figure 3 shows examples of synthesized images with 3DGS [28], RegNeRF [40], and Instant-NGP [38], with and without our method. As already seen in the quantitative results (Section 4.2), the output quality of the proposed Re-Nerfing improves significantly upon the baselines, especially in terms of the reduction of floating artifacts. In particular, the addition of our method sharpens the scene and better preserves the small details as can be seen for RegNeRF in Figure 3. Remarkably, the proposed method is able to remove dominant artifacts in the renderings by Instant-NGP and 3DGS, despite using the same original views, architecture, and hyperparameters as the baselines. The augmented views help disambiguating the scene geometry, allowing all models to deliver better results by converging to a better solution.

The **supplementary material** includes additional details and results, such as the performance on each scene and extra qualitative examples in a video. There we also show how the proposed Re-Nerfing can densify the SfM point cloud that can be used to initialize 3DGS.

**Limitations** Our method relies on the first stage to pro-

vide reasonable renderings and a decent estimate of the scene geometry, so it is challenging to enhance poorly rendered scenes, e.g., the *stump* scene with Instant-NGP [38], which could not converge. The proposed method also relies on the uncertainty estimates to discard artifacts and low-quality areas. Therefore, better uncertainty estimates would be beneficial. Uncertainty calibration of the threshold  $\mu$  could help refine the estimates while preserving the signal in higher-quality areas.

### 5. Conclusion

This work enhances NeRFs and 3DGSs by leveraging their own novel view synthesis capabilities. The introduced Re-Nerfing is a general approach that synthesizes novel views to improve the scene coverage and augment the training data for a new model. To provide a valuable training signal for the second model, Re-Nerfing computes the NeRF’s uncertainty for each augmented view to discard the uncertain regions and reduce artifacts. As shown with various pipelines, our method yields improvements in both reconstruction and rendering quality in sparse scenes, mitigating the need for extensive captures of the scene.

# Re-Nerfing: Improving Novel View Synthesis through Novel View Synthesis

## Supplementary Material

### A. Appendix

In this supplementary material, we complement the main paper with additional details and results. Specifically, we illustrate and discuss the trade-offs due to the synthetic view poses (Section A.1), we experiment with and discuss the impact of our method on the SfM point cloud (Section A.2), we present the result in dense-view settings (Section A.3), we discuss an extra ablation study (Section A.4), we show more qualitative results, also through a video (Section A.5), and we present the quantitative results by scene (Section A.6).

#### A.1. More on the Views Positioning Trade-Offs

In Figure 5, we illustrate the trade-offs associated with the relative positioning between the original views and the synthesized ones. Considering two existing views, the quality of the views synthesized between them varies as follows: the closer the synthetic views are to the original views, the higher their quality because the viewpoint change is small. Instead, the further from the original views (e.g., towards 0.5), the worse the quality becomes (e.g., more artifacts) as the viewpoint shift is more significant and the uncertainty increases. However, synthesizing views only in the vicinity of the original ones is not particularly beneficial as the views are too similar to the original ones and, as such, do not help disambiguate the scene geometry. Therefore, the views should also be synthesized at further locations. With Re-Nerfing, to mitigate the quality degradation, we remove the artifacts within the synthesized views (i.e., occurring more at the further poses) by filtering out the uncertain regions. This allows us to synthesize many views throughout the interpolated poses. We sample more poses closer to the

Method	PSNR	SSIM	LPIPS
Instant-NGP [38]	25.87	0.812	0.162
+ Re-Nerfing [ours]	<b>25.88</b>	<b>0.814</b>	<b>0.161</b>
PyNeRF [59]	27.41	0.874	0.094
+ Re-Nerfing [ours]	<b>27.43</b>	<b>0.875</b>	<b>0.093</b>
3DGS [28]	27.83	0.855	<b>0.109</b>
+ Re-Nerfing [ours]	<b>28.03</b>	<b>0.859</b>	0.111

Table 6. Rendering performance on the mip-NeRF 360 [3] dataset in **dense view settings** averaged over the scenes. The proposed Re-Nerfing is applied on the Instant-NGP [38], PyNeRF [59], and 3DGS [28] baselines, using the corresponding baseline to augment the views. Uncertainty estimates are unavailable for 3DGS.

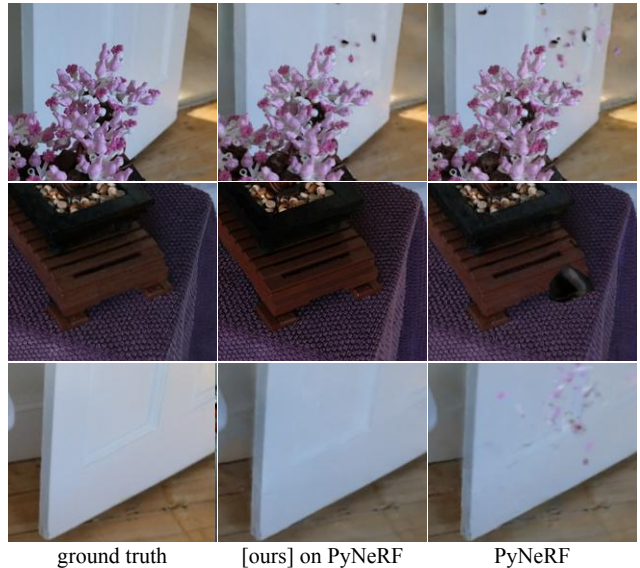


Figure 4. Qualitative results on cropped images from the test set of the mip-NeRF 360 dataset [3] showcasing PyNeRF [59] in sparse-view settings, with and without the proposed Re-Nerfing.

original views (i.e., 0.0 and 1.0) and fewer poses in the middle. Specifically, we synthesize in the 7x configuration at the interpolation factors 0.1, 0.2, 0.4, 0.6, 0.8, and 0.9. This trade-off is explored in Table 4.

#### A.2. Impact on the SfM Point Cloud

In Table 7, we investigate the impact of Re-Nerfing on the SfM point cloud. For these experiments, we used 3DGS [28] initialized with the SfM point cloud constructed by the SfM pipeline of Nerfstudio [56] using Hloc [50] and Superpoint [16] from the sparse settings. For the second stage of Re-Nerfing, we followed the same protocol of Section 3 but ran the aforementioned SfM-pipeline on the synthetic and real images combined. Remarkably, despite synthetic views, not only did Re-Nerfing improve over the standard 3DGS but also densified the point cloud by a substantial 4.6x on average. This significant difference in the number of points (# points) is evidence of the effectiveness of NVS and Re-Nerfing to aid and simplify the triangulation of the scene geometry, which is the foundation of our work. In particular, the *bicycle* scene has more points than the other ones because of its higher image resolution. Thanks to a much denser point cloud as initialization and the added synthesized views, the proposed Re-Nerfing reaches a better solution, as shown by the metrics.

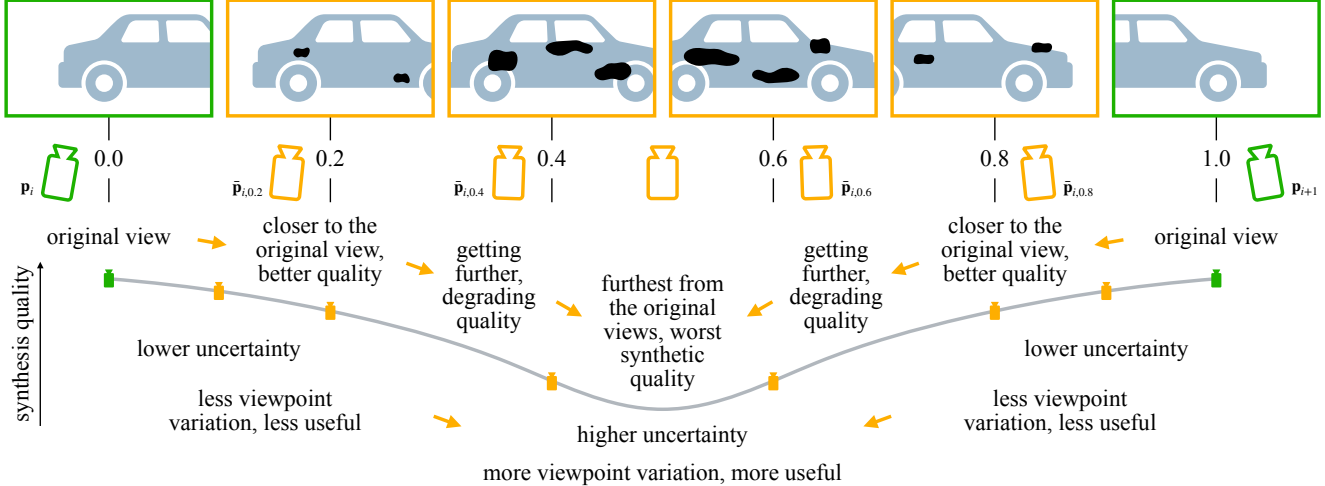


Figure 5. Illustration of the trade-offs arising when synthesizing novel views (orange) in between existing ones (green). The numbers indicate the interpolation factors. The closer to the original views, the higher the quality of the synthesis and the lower the uncertainty. Moving further from the original views (i.e., toward 0.5), the quality degrades and the uncertainty increases. Yet, an opposite trade-off occurs as views too close to the original ones do not bring any extra information. We balance this by using many views and removing artifacts thanks to the uncertainty estimates.

Scene - <i>sparse</i>	3DGS [28] (SfM, Hloc+Superpoint)				Re-Nerfing (SfM, Hloc+Superpoint)			
	PSNR	SSIM	LPIPS	# Points	PSNR	SSIM	LPIPS	# Points
<i>bonsai</i>	26.19	0.847	0.131	6683	26.52	0.864	0.126	20274
<i>counter</i>	23.29	0.766	0.167	8032	23.32	0.773	0.165	30855
<i>kitchen</i>	24.27	0.849	0.098	3914	24.22	0.852	0.099	13716
<i>room</i>	24.82	0.829	0.162	4304	24.73	0.833	0.167	16216
<i>garden</i>	24.33	0.773	0.089	4873	24.87	0.793	0.081	13646
<i>stump</i>	21.97	0.528	0.230	7337	22.36	0.568	0.228	38891
<i>bicycle</i>	20.04	0.482	0.329	18831	20.38	0.514	0.301	114554
average	23.56	0.725	0.172	7711	<b>23.77</b>	<b>0.742</b>	<b>0.167</b>	<b>35450</b>

Table 7. Impact of Re-Nerfing on the SfM point cloud and 3DGS [28] initialized with it. SfM is run for all with HLoc [50] with Superpoint [16] features. For Re-Nerfing, SfM is run with the synthesized views, too.

### A.3. Dense-View Settings

Throughout this work, we experimented with challenging sparse-view settings. There, the limited views available prevent a good triangulation of the scene geometry. In Table 6, we show the impact of our Re-Nerfing on Instant-NGP [38], PyNeRF [59], and 3DGS [28] in dense-view settings. Therefore, in these experiments, we use all the available training views. Remarkably, despite the already many views available, by adding synthesized ones, the proposed Re-Nerfing does not degrade the performance and even slightly improves it. Nearly equal results are seen for Instant-NGP and PyNeRF, while a +0.2db PSNR is brought over 3DGS. This shows the flexibility of Re-Nerfing.

### A.4. Additional Ablation Study

In Table 8, we report an ablation study for both PyNeRF [59] and Instant-NGP [38] in the 30-view setting. Training again with the synthetic views produced by the baseline (with  $N = 7$ ) slightly degrades the performance for all metrics for PyNeRF, while it improves for Instant-NGP. The degradation for PyNeRF is due to the lower quality signal of 6x more views than the reliable signal of the original views. Specifically, the model learns the artifacts of the augmented views and underperforms. Instead, for Instant-NGP, the quality of the augmented views was higher, leading to improvements. Nevertheless, removing the images from the sampling pool once the scene structure has been mainly learned (stop, 3rd row) prevents both mod-

Method	PyNeRF [59]			Instant-NGP [38]		
	PSNR	SSIM	LPIPS	PSNR	SSIM	LPIPS
baseline	23.16	0.840	0.119	20.75	0.709	0.232
+ augmented views	23.08	0.829	0.125	21.54	0.740	0.208
+ stop aug. views	23.84	0.862	0.102	21.57	0.743	0.201
+ masks	<b>24.08</b>	<b>0.872</b>	<b>0.099</b>	<b>21.70</b>	<b>0.753</b>	<b>0.195</b>

Table 8. Ablation on the mip-NeRF 360 [3] dataset in the sparser settings of the *kitchen* scene (30 views). The proposed Re-Nerfing is applied on Instant-NGP [38] and PyNeRF [59], using the corresponding baseline to augment the views.

els from overfitting to the artifacts and leads to better results on all metrics, with large improvements for PyNeRF. Furthermore, masking out the uncertain regions of such synthetic views improves even further across the board for both methods. This shows once again how synthetic views of the same scene are beneficial aid the novel view synthesis task. In particular, the results confirm the importance of increasing the scene coverage and that of having a good training signal, testifying the need for the uncertainty-based masks and our augmentation strategy.

### A.5. Additional Qualitative Results

**PyNeRF** In Figure 4, we showcase the impact of our method on PyNeRF [59]. As for the other methods seen in the main paper, our Re-Nerfing reduces artifacts and leads to a better solution, e.g., by removing floaters. Examples are the floating leaves of the bonsai (first and last rows), or the black blob (second row).

**Video** We refer to the attached supplementary video for more qualitative results. The video interpolates across the test views for models trained in sparse settings. Remarkably, when paired with the proposed Re-Nerfing 3DGS [28] reaches significantly higher rendering quality in the *counter* scene (30 views). Thanks to our method, the scene geometry is substantially better captured by the Gaussians, eliminating major structural artifacts. As shown in Table 20, the *garden* scene is easier to render. In this case, our method helps with the scene geometry, especially visible in the rendered depths, as it eliminates the holes in the ground.

### A.6. Evaluation by Scene

**LLFF** In Tables from 9 to 16, we report the performance for each scene in the 3-view setting of LLFF [36] for RegNeRF [40] and Re-Nerfing. The detailed results showcase that the proposed method always improves upon RegNeRF, while the performance sometimes saturates before 3 rounds.

**mip-NeRF 360** In Tables from 17 to 23, we report the performance for each scene for the various pipelines on which we applied Re-Nerfing, namely Instant-NGP [38], PyNeRF [59], and 3D Gaussian Splatting [28]. The detailed results showcase the benefits of our method indoor

<i>fortress</i> , 3 views	PSNR	SSIM	LPIPS
RegNeRF [40]	23.32	0.743	0.065
+ Re-Nerfing, 1 round [ours]	23.69	0.789	0.054
+ extra round, 2nd [ours]	23.94	0.814	0.047
+ extra round, 3rd [ours]	<b>24.34</b>	<b>0.829</b>	<b>0.046</b>

Table 9. Results on the *fortress* scene of the LLFF dataset [36] for the **3-view** settings. The proposed Re-Nerfing is applied on RegNeRF [40] and then to itself iteratively (rounds).

<i>horns</i> , 3 views	PSNR	SSIM	LPIPS
RegNeRF [40]	15.65	0.610	0.200
+ Re-Nerfing, 1 round [ours]	15.75	0.654	0.179
+ extra round, 2nd [ours]	15.80	0.655	0.168
+ extra round, 3rd [ours]	<b>16.68</b>	<b>0.670</b>	<b>0.161</b>

Table 10. Results on the *horns* scene of the LLFF dataset [36] for the **3-view** settings. The proposed Re-Nerfing is applied on RegNeRF [40] and then to itself iteratively (rounds).

<i>fern</i> , 3 views	PSNR	SSIM	LPIPS
RegNeRF [40]	19.87	0.697	0.202
+ Re-Nerfing, 1 round [ours]	<b>19.96</b>	0.709	0.191
+ extra round, 2nd [ours]	<b>19.96</b>	0.714	<b>0.180</b>
+ extra round, 3rd [ours]	19.95	<b>0.718</b>	<b>0.180</b>

Table 11. Results on the *fern* scene of the LLFF dataset [36] for the **3-view** settings. The proposed Re-Nerfing is applied on RegNeRF [40] and then to itself iteratively (rounds).

and outdoor, for sparser and denser view settings, and for both implicit and explicit methods.

<i>flower</i> , 3 views	PSNR	SSIM	LPIPS
RegNeRF [40]	19.93	0.688	0.156
+ Re-Nerfing, 1 round [ours]	20.28	0.711	0.143
+ extra round, 2nd [ours]	<b>20.46</b>	<b>0.720</b>	<b>0.140</b>
+ extra round, 3rd [ours]	20.04	0.695	0.154

Table 12. Results on the *flower* scene of the LLFF dataset [36] for the **3-view** settings. The proposed Re-Nerfing is applied on RegNeRF [40] and then to itself iteratively (rounds).

<i>orchids</i> , 3 views	PSNR	SSIM	LPIPS
RegNeRF [40]	15.56	0.502	0.177
+ Re-Nerfing, 1 round [ours]	15.77	0.526	0.162
+ extra round, 2nd [ours]	15.86	0.540	0.155
+ extra round, 3rd [ours]	<b>15.90</b>	<b>0.547</b>	<b>0.150</b>

Table 13. Results on the *orchids* scene of the LLFF dataset [36] for the **3-view** settings. The proposed Re-Nerfing is applied on RegNeRF [40] and then to itself iteratively (rounds).

<i>leaves</i> , 3 views	PSNR	SSIM	LPIPS
RegNeRF [40]	16.60	0.612	0.132
+ Re-Nerfing, 1 round [ours]	16.92	0.654	0.116
+ extra round, 2nd [ours]	17.07	0.670	0.107
+ extra round, 3rd [ours]	<b>17.14</b>	<b>0.677</b>	<b>0.103</b>

Table 14. Results on the *leaves* scene of the LLFF dataset [36] for the **3-view** settings. The proposed Re-Nerfing is applied on RegNeRF [40] and then to itself iteratively (rounds).

<i>room</i> , 3 views	PSNR	SSIM	LPIPS
RegNeRF [40]	21.53	0.861	0.116
+ Re-Nerfing, 1 round [ours]	21.84	0.873	0.105
+ extra round, 2nd [ours]	<b>21.96</b>	<b>0.878</b>	<b>0.098</b>
+ extra round, 3rd [ours]	21.47	0.871	0.107

Table 15. Results on the *room* scene of the LLFF dataset [36] for the **3-view** settings. The proposed Re-Nerfing is applied on RegNeRF [40] and then to itself iteratively (rounds).

<i>t-rex</i> , 3 views	PSNR	SSIM	LPIPS
RegNeRF [40]	20.16	0.766	0.133
+ Re-Nerfing, 1 round [ours]	20.55	0.788	0.117
+ extra round, 2nd [ours]	<b>20.70</b>	<b>0.797</b>	<b>0.111</b>
+ extra round, 3rd [ours]	20.63	0.796	0.113

Table 16. Results on the *t-rex* scene of the LLFF dataset [36] for the **3-view** settings. The proposed Re-Nerfing is applied on RegNeRF [40] and then to itself iteratively (rounds).

Method	<i>counter</i> - sparser			<i>counter</i> - denser		
	PSNR	SSIM	LPIPS	PSNR	SSIM	LPIPS
Instant-NGP [38]	17.72	0.557	0.458	<b>25.52</b>	0.801	0.183
+ Re-Nerfing [ours]	<b>17.97</b>	<b>0.573</b>	<b>0.422</b>	25.50	<b>0.805</b>	<b>0.180</b>
PyNeRF [59]	17.57	0.643	0.325	26.80	0.864	0.111
+ Re-Nerfing [ours]	<b>18.09</b>	<b>0.676</b>	<b>0.299</b>	<b>27.13</b>	<b>0.871</b>	<b>0.107</b>
3DGS [28]	19.31	0.609	0.296	27.69	<b>0.886</b>	<b>0.119</b>
+ Re-Nerfing [ours]	<b>21.08</b>	<b>0.686</b>	<b>0.241</b>	<b>27.70</b>	0.879	0.127

Table 17. Results on the *counter* scene of the mip-NeRF 360 dataset [3], for sparser and denser settings. The proposed Re-Nerfing is applied on Instant-NGP [38], PyNeRF [59], and 3DGS [28]. Uncertainty estimates are unavailable for 3DGS.

Method	<i>bicycle</i> - sparser			<i>bicycle</i> - denser		
	PSNR	SSIM	LPIPS	PSNR	SSIM	LPIPS
Instant-NGP [38]	20.98	0.477	0.370	23.30	0.625	0.301
+ Re-Nerfing [ours]	<b>21.27</b>	<b>0.499</b>	<b>0.345</b>	<b>23.35</b>	<b>0.630</b>	<b>0.300</b>
PyNeRF [59]	22.13	0.608	0.234	24.92	0.779	0.154
+ Re-Nerfing [ours]	<b>22.96</b>	<b>0.643</b>	<b>0.200</b>	<b>25.19</b>	<b>0.784</b>	<b>0.150</b>
3DGS [28]	17.48	0.320	0.403	25.37	<b>0.775</b>	<b>0.136</b>
+ Re-Nerfing [ours]	<b>18.36</b>	<b>0.324</b>	<b>0.377</b>	<b>25.39</b>	0.774	0.149

Table 18. Results on the *bicycle* scene of the mip-NeRF 360 dataset [3], for sparser and denser settings. The proposed Re-Nerfing is applied on Instant-NGP [38], PyNeRF [59], and 3DGS [28]. Uncertainty estimates are unavailable for 3DGS.

Method	<i>stump</i> - sparser			<i>stump</i> - denser		
	PSNR	SSIM	LPIPS	PSNR	SSIM	LPIPS
PyNeRF [59]	22.42	0.632	0.218	26.47	0.810	0.117
+ Re-Nerfing [ours]	<b>23.75</b>	<b>0.672</b>	<b>0.188</b>	<b>26.51</b>	<b>0.814</b>	<b>0.112</b>
3DGS [28]	19.72	0.409	0.311	23.81	0.666	0.177
+ Re-Nerfing [ours]	<b>19.97</b>	<b>0.433</b>	<b>0.306</b>	<b>24.32</b>	<b>0.691</b>	<b>0.172</b>

Table 19. Results on the *stump* scene of the mip-NeRF 360 dataset [3], for sparser and denser settings. The proposed Re-Nerfing is applied on PyNeRF [59] and 3DGS [28]. Instant-NGP [38] could not deal with this scene in the sparser setting (PSNR of 15.55), so it was not applied here. Uncertainty estimates are unavailable for 3DGS.

Method	<i>garden</i> - sparser			<i>garden</i> - denser		
	PSNR	SSIM	LPIPS	PSNR	SSIM	LPIPS
Instant-NGP [38]	23.03	0.733	0.163	25.54	0.829	0.111
+ Re-Nerfing [ours]	<b>23.27</b>	<b>0.743</b>	<b>0.149</b>	<b>25.64</b>	<b>0.831</b>	<b>0.108</b>
PyNeRF [59]	25.80	0.841	0.073	<b>28.26</b>	<b>0.900</b>	<b>0.052</b>
+ Re-Nerfing [ours]	<b>26.18</b>	<b>0.845</b>	<b>0.071</b>	27.88	0.897	0.055
3DGS [28]	21.97	0.670	0.140	27.44	0.889	0.063
+ Re-Nerfing [ours]	<b>23.18</b>	<b>0.730</b>	<b>0.106</b>	<b>27.93</b>	<b>0.900</b>	<b>0.048</b>

Table 20. Results on the *garden* scene of the mip-NeRF 360 dataset [3], for sparser and denser settings. The proposed Re-Nerfing is applied on Instant-NGP [38], PyNeRF [59], and 3DGS [28]. Uncertainty estimates are unavailable for 3DGS.

Method	<i>bonsai</i> - sparser			<i>bonsai</i> - denser		
	PSNR	SSIM	LPIPS	PSNR	SSIM	LPIPS
Instant-NGP [38]	19.41	0.699	0.335	<b>26.96</b>	<b>0.894</b>	<b>0.098</b>
+ Re-Nerfing [ours]	<b>19.78</b>	<b>0.711</b>	<b>0.310</b>	26.77	0.892	0.100
PyNeRF [59]	23.61	0.837	0.137	<b>29.40</b>	<b>0.932</b>	<b>0.063</b>
+ Re-Nerfing [ours]	<b>24.70</b>	<b>0.854</b>	<b>0.118</b>	29.37	0.931	<b>0.063</b>
3DGS [28]	<b>23.32</b>	<b>0.743</b>	<b>0.212</b>	<b>30.88</b>	<b>0.938</b>	<b>0.078</b>
+ Re-Nerfing [ours]	23.09	0.705	0.217	30.61	0.931	0.087

Table 21. Results on the *bonsai* scene of the mip-NeRF 360 dataset [3], for sparser and denser settings. The proposed Re-Nerfing is applied on Instant-NGP [38], PyNeRF [59], and 3DGS [28]. Uncertainty estimates are unavailable for 3DGS.

Method	<i>kitchen</i> - sparser			<i>kitchen</i> - denser		
	PSNR	SSIM	LPIPS	PSNR	SSIM	LPIPS
Instant-NGP [38]	20.75	0.709	0.232	<b>26.28</b>	0.837	<b>0.135</b>
+ Re-Nerfing [ours]	<b>21.70</b>	<b>0.753</b>	<b>0.195</b>	25.97	<b>0.839</b>	0.136
PyNeRF [59]	23.16	0.840	0.119	<b>28.77</b>	<b>0.919</b>	<b>0.069</b>
+ Re-Nerfing [ours]	<b>24.08</b>	<b>0.872</b>	<b>0.099</b>	28.62	0.916	0.073
3DGS [28]	21.95	0.770	0.149	30.13	<b>0.928</b>	<b>0.062</b>
+ Re-Nerfing [ours]	<b>22.56</b>	<b>0.797</b>	<b>0.130</b>	<b>30.21</b>	<b>0.928</b>	0.064

Table 22. Results on the *kitchen* scene of the mip-NeRF 360 dataset [3], for sparser and denser settings. The proposed Re-Nerfing is applied on Instant-NGP [38], PyNeRF [59], and 3DGS [28]. Uncertainty estimates are unavailable for 3DGS.

Method	<i>room</i> - sparser			<i>room</i> - denser		
	PSNR	SSIM	LPIPS	PSNR	SSIM	LPIPS
Instant-NGP [38]	22.68	0.778	0.248	27.62	0.883	0.143
+ Re-Nerfing [ours]	<b>24.14</b>	<b>0.801</b>	<b>0.217</b>	<b>28.07</b>	<b>0.886</b>	<b>0.139</b>
PyNeRF [59]	23.85	0.825	0.168	27.24	<b>0.913</b>	0.092
+ Re-Nerfing [ours]	<b>24.81</b>	<b>0.841</b>	<b>0.146</b>	<b>27.28</b>	0.911	<b>0.091</b>
3DGS [28]	19.67	0.677	0.301	29.50	0.903	0.129
+ Re-Nerfing [ours]	<b>20.89</b>	<b>0.715</b>	<b>0.271</b>	<b>30.02</b>	<b>0.907</b>	<b>0.128</b>

Table 23. Results on the *room* scene of the mip-NeRF 360 dataset [3], for sparser and denser settings. The proposed Re-Nerfing is applied on Instant-NGP [38], PyNeRF [59], and 3DGS [28]. Uncertainty estimates are unavailable for 3DGS.

## References

- [1] Young Chun Ahn, Seokhwan Jang, Sungheon Park, Ji-Yeon Kim, and Nahyup Kang. PANeRF: Pseudo-view augmentation for improved neural radiance fields based on few-shot inputs. *arXiv preprint arXiv:2211.12758*, 2022. 3
- [2] Jonathan T Barron, Ben Mildenhall, Matthew Tancik, Peter Hedman, Ricardo Martin-Brualla, and Pratul P Srinivasan. Mip-NeRF: A multiscale representation for anti-aliasing neural radiance fields. In *Proceedings of the IEEE/CVF International Conference on Computer Vision*, pages 5855–5864, 2021. 1, 2, 6
- [3] Jonathan T Barron, Ben Mildenhall, Dor Verbin, Pratul P Srinivasan, and Peter Hedman. Mip-NeRF 360: Unbounded anti-aliased neural radiance fields. In *Proceedings of the IEEE/CVF Conference on Computer Vision and Pattern Recognition*, pages 5470–5479, 2022. 1, 2, 5, 6, 7, 3
- [4] Wenjing Bian, Zirui Wang, Kejie Li, Jia-Wang Bian, and Victor Adrian Prisacariu. Nope-NeRF: Optimising neural radiance field with no pose prior. In *Proceedings of the IEEE/CVF Conference on Computer Vision and Pattern Recognition*, pages 4160–4169, 2023. 1, 2
- [5] Matteo Bortolon, Alessio Del Bue, and Fabio Poiesi. VM-NeRF: Tackling sparsity in NeRF with view morphing. In *Proceedings of the International Conference on Image Analysis and Processing*, pages 63–74. Springer, 2023. 3
- [6] James Bradbury, Roy Frostig, Peter Hawkins, Matthew James Johnson, Chris Leary, Dougal Maclaurin, George Necula, Adam Paszke, Jake VanderPlas, Skye Wanderman-Milne, and Qiao Zhang. JAX: composable transformations of Python+NumPy programs, 2018. 6
- [7] Ang Cao and Justin Johnson. HexPlane: A fast representation for dynamic scenes. In *Proceedings of the IEEE/CVF Conference on Computer Vision and Pattern Recognition*, pages 130–141, 2023. 2
- [8] Anpei Chen, Zexiang Xu, Andreas Geiger, Jingyi Yu, and Hao Su. Tensorf: Tensorial radiance fields. In *Proceedings of the European Conference on Computer Vision*. Springer, 2022. 2
- [9] Di Chen, Yu Liu, Lianghua Huang, Bin Wang, and Pan Pan. GeoAug: Data augmentation for few-shot nerf with geometry constraints. In *Proceedings of the European Conference on Computer Vision*, pages 322–337. Springer, 2022. 3
- [10] Liang-Chieh Chen, Raphael Gontijo Lopes, Bowen Cheng, Maxwell D Collins, Ekin D Cubuk, Barret Zoph, Hartwig Adam, and Jonathon Shlens. Naive-student: Leveraging semi-supervised learning in video sequences for urban scene segmentation. In *Proceedings of the European Conference on Computer Vision*, pages 695–714. Springer, 2020. 3, 7
- [11] Tianlong Chen, Peihao Wang, Zhiwen Fan, and Zhangyang Wang. Aug-NeRF: Training stronger neural radiance fields with triple-level physically-grounded augmentations. In *Proceedings of the IEEE/CVF Conference on Computer Vision and Pattern Recognition*, pages 15191–15202, 2022. 3
- [12] Zhiqin Chen, Thomas Funkhouser, Peter Hedman, and Andrea Tagliasacchi. MobileNeRF: Exploiting the polygon rasterization pipeline for efficient neural field rendering on mobile architectures. In *Proceedings of the IEEE/CVF Conference on Computer Vision and Pattern Recognition*, pages 16569–16578, 2023. 1
- [13] Inchang Choi, Orazio Gallo, Alejandro Troccoli, Min H Kim, and Jan Kautz. Extreme view synthesis. In *Proceedings of the IEEE/CVF International Conference on Computer Vision*, pages 7781–7790, 2019. 2
- [14] Thomas Cover and Peter Hart. Nearest neighbor pattern classification. *Transactions on Information Theory*, 13(1):21–27, 1967. 4
- [15] Kangle Deng, Andrew Liu, Jun-Yan Zhu, and Deva Ramanan. Depth-supervised NeRF: Fewer views and faster training for free. In *Proceedings of the IEEE/CVF Conference on Computer Vision and Pattern Recognition*, pages 12882–12891, 2022. 1, 2, 4
- [16] Daniel DeTone, Tomasz Malisiewicz, and Andrew Rabynovich. Superpoint: Self-supervised interest point detection and description. In *Proceedings of the IEEE conference on computer vision and pattern recognition workshops*, pages 224–236, 2018. 1, 2
- [17] Zhiwen Fan, Wenyan Cong, Kairun Wen, Kevin Wang, Jian Zhang, Xinghao Ding, Danfei Xu, Boris Ivanovic, Marco Pavone, Georgios Pavlakos, et al. Instantsplat: Unbounded sparse-view pose-free gaussian splatting in 40 seconds. *arXiv preprint arXiv:2403.20309*, 2024. 2
- [18] Casimir Feldmann, Niall Siegenheim, Nikolas Hars, Lovro Rabuzin, Mert Ertugrul, Luca Wolfart, Marc Pollefeys, Zuria Bauer, and Martin R Oswald. NeRFmentation: NeRF-based augmentation for monocular depth estimation. *arXiv preprint arXiv:2401.03771*, 2024. 3
- [19] John Flynn, Ivan Neulander, James Philbin, and Noah Snavely. DeepStereo: Learning to predict new views from the world’s imagery. In *Proceedings of the IEEE Conference on Computer Vision and Pattern Recognition*, pages 5515–5524, 2016. 2
- [20] Sara Fridovich-Keil, Alex Yu, Matthew Tancik, Qinhong Chen, Benjamin Recht, and Angjoo Kanazawa. Plenoxels: Radiance fields without neural networks. In *Proceedings of the IEEE/CVF Conference on Computer Vision and Pattern Recognition*, pages 5501–5510, 2022. 2
- [21] Sara Fridovich-Keil, Giacomo Meanti, Frederik Rahbæk Warburg, Benjamin Recht, and Angjoo Kanazawa. K-planes: Explicit radiance fields in space, time, and appearance. In *Proceedings of the IEEE/CVF Conference on Computer Vision and Pattern Recognition*, pages 12479–12488, 2023. 2
- [22] Stephan J Garbin, Marek Kowalski, Matthew Johnson, Jamie Shotton, and Julien Valentin. FastNeRF: High-fidelity neural rendering at 200FPS. In *Proceedings of the IEEE/CVF International Conference on Computer Vision*, pages 14346–14355, 2021. 2
- [23] Stefano Gasperini, Nils Morbitzer, HyunJun Jung, Nassir Navab, and Federico Tombari. Robust monocular depth estimation under challenging conditions. In *Proceedings of the IEEE/CVF International Conference on Computer Vision*, pages 8177–8186, 2023. 3, 7
- [24] Golnaz Ghiasi, Yin Cui, Aravind Srinivas, Rui Qian, Tsung-Yi Lin, Ekin D Cubuk, Quoc V Le, and Barret Zoph. Simple copy-paste is a strong data augmentation method for instance

- segmentation. In *Proceedings of the IEEE/CVF Conference on Computer Vision and Pattern Recognition*, pages 2918–2928, 2021. 3
- [25] Lily Goli, Cody Reading, Silvia Sellán, Alec Jacobson, and Andrea Tagliasacchi. Bayes’ Rays: Uncertainty quantification for neural radiance fields. *arXiv preprint arXiv:2309.03185*, 2023. 5, 6
- [26] Geoffrey Hinton, Oriol Vinyals, and Jeff Dean. Distilling the knowledge in a neural network. *arXiv preprint arXiv:1503.02531*, 2015. 3
- [27] Kacper Kania, Kwang Moo Yi, Marek Kowalski, Tomasz Trzcíński, and Andrea Tagliasacchi. CoNeRF: Controllable neural radiance fields. In *Proceedings of the IEEE/CVF Conference on Computer Vision and Pattern Recognition*, pages 18623–18632, 2022. 2
- [28] Bernhard Kerbl, Georgios Kopanas, Thomas Leimkühler, and George Drettakis. 3D Gaussian splatting for real-time radiance field rendering. *ACM Transactions on Graphics*, 42(4):1–14, 2023. 1, 2, 3, 4, 6, 7, 8, 5
- [29] Abhijit Kundu, Kyle Genova, Xiaoqi Yin, Alireza Fathi, Caroline Pantofaru, Leonidas J Guibas, Andrea Tagliasacchi, Frank Dellaert, and Thomas Funkhouser. Panoptic neural fields: A semantic object-aware neural scene representation. In *Proceedings of the IEEE/CVF Conference on Computer Vision and Pattern Recognition*, pages 12871–12881, 2022. 2
- [30] Alexander Lehner, Stefano Gasperini, Alvaro Marcos-Ramiro, Michael Schmidt, Nassir Navab, Benjamin Busam, and Federico Tombari. 3D adversarial augmentations for robust out-of-domain predictions. *International Journal of Computer Vision*, pages 1–33, 2023. 3
- [31] Marc Levoy and Pat Hanrahan. Light field rendering. In *Proceedings of the Conference on Computer Graphics and Interactive Techniques*, page 31–42. Association for Computing Machinery, 1996. 2
- [32] Jiahe Li, Jiawei Zhang, Xiao Bai, Jin Zheng, Xin Ning, Jun Zhou, and Lin Gu. Dngaussian: Optimizing sparse-view 3d gaussian radiance fields with global-local depth normalization. In *Proceedings of the IEEE/CVF Conference on Computer Vision and Pattern Recognition*, pages 20775–20785, 2024. 2
- [33] Chen-Hsuan Lin, Wei-Chiu Ma, Antonio Torralba, and Simon Lucey. BARF: Bundle-adjusting neural radiance fields. In *Proceedings of the IEEE/CVF International Conference on Computer Vision*, pages 5741–5751, 2021. 1, 2
- [34] Ricardo Martin-Brualla, Noha Radwan, Mehdi SM Sajjadi, Jonathan T Barron, Alexey Dosovitskiy, and Daniel Duckworth. NeRF in the wild: Neural radiance fields for unconstrained photo collections. In *Proceedings of the IEEE/CVF Conference on Computer Vision and Pattern Recognition*, pages 7210–7219, 2021. 1
- [35] Lars Mescheder, Michael Oechsle, Michael Niemeyer, Sebastian Nowozin, and Andreas Geiger. Occupancy networks: Learning 3d reconstruction in function space. In *Proceedings of the IEEE/CVF Conference on Computer Vision and Pattern Recognition (CVPR)*, 2019. 2
- [36] Ben Mildenhall, Pratul P Srinivasan, Rodrigo Ortiz-Cayon, Nima Khademi Kalantari, Ravi Ramamoorthi, Ren Ng, and Abhishek Kar. Local Light Field Fusion: Practical view synthesis with prescriptive sampling guidelines. *ACM Transactions on Graphics (ToG)*, 38(4):1–14, 2019. 1, 2, 5, 6, 3, 4
- [37] Ben Mildenhall, Pratul P Srinivasan, Matthew Tancik, Jonathan T Barron, Ravi Ramamoorthi, and Ren Ng. NeRF: Representing scenes as neural radiance fields for view synthesis. In *Proceedings of the European Conference on Computer Vision*, pages 405–421. Springer, 2020. 1, 2, 3
- [38] Thomas Müller, Alex Evans, Christoph Schied, and Alexander Keller. Instant neural graphics primitives with a multiresolution hash encoding. *ACM Transactions on Graphics (ToG)*, 41(4):1–15, 2022. 1, 2, 6, 8, 3, 5, 7
- [39] Alexey Nekrasov, Jonas Schult, Or Litany, Bastian Leibe, and Francis Engelmann. Mix3D: Out-of-context data augmentation for 3D scenes. In *Proceedings of the International Conference on 3D Vision (3DV)*, pages 116–125. IEEE, 2021. 3
- [40] Michael Niemeyer, Jonathan T Barron, Ben Mildenhall, Mehdi SM Sajjadi, Andreas Geiger, and Noha Radwan. Regnerf: Regularizing neural radiance fields for view synthesis from sparse inputs. In *Proceedings of the IEEE/CVF Conference on Computer Vision and Pattern Recognition*, pages 5480–5490, 2022. 1, 2, 4, 5, 6, 8, 3
- [41] Avinash Paliwal, Wei Ye, Jinhui Xiong, Dmytro Kotovenko, Rakesh Ranjan, Vikas Chandra, and Nima Khademi Kalantari. Coherentgs: Sparse novel view synthesis with coherent 3d gaussians. *arXiv preprint arXiv:2403.19495*, 2024. 2
- [42] Jeong Joon Park, Peter Florence, Julian Straub, Richard Newcombe, and Steven Lovegrove. DeepSDF: Learning continuous signed distance functions for shape representation. In *Proceedings of the IEEE/CVF Conference on Computer Vision and Pattern Recognition (CVPR)*, 2019. 2
- [43] Keunhong Park, Utkarsh Sinha, Jonathan T Barron, Sofien Bouaziz, Dan B Goldman, Steven M Seitz, and Ricardo Martin-Brualla. Nerfies: Deformable neural radiance fields. In *Proceedings of the IEEE/CVF International Conference on Computer Vision*, pages 5865–5874, 2021. 2
- [44] Keunhong Park, Utkarsh Sinha, Peter Hedman, Jonathan T. Barron, Sofien Bouaziz, Dan B Goldman, Ricardo Martin-Brualla, and Steven M. Seitz. HyperNeRF: A higher-dimensional representation for topologically varying neural radiance fields. *ACM Transactions on Graphics (ToG)*, 40(6), 2021. 2
- [45] Keunhong Park, Philipp Henzler, Ben Mildenhall, Jonathan T Barron, and Ricardo Martin-Brualla. CamP: Camera preconditioning for neural radiance fields. *ACM Transactions on Graphics (TOG)*, 42(6):1–11, 2023. 2
- [46] Charles R Qi, Hao Su, Kaichun Mo, and Leonidas J Guibas. PointNet: Deep learning on point sets for 3d classification and segmentation. In *Proceedings of the IEEE Conference on Computer Vision and Pattern Recognition*, pages 652–660, 2017. 2
- [47] Daniel Rebain, Mark Matthews, Kwang Moo Yi, Dmitry Lagun, and Andrea Tagliasacchi. LOLNeRF: Learn from one look. In *Proceedings of the IEEE/CVF Conference on Computer Vision and Pattern Recognition*, pages 1558–1567, 2022. 2

- [48] Konstantinos Rematas, Andrew Liu, Pratul P Srinivasan, Jonathan T Barron, Andrea Tagliasacchi, Thomas Funkhouser, and Vittorio Ferrari. Urban radiance fields. In *Proceedings of the IEEE/CVF Conference on Computer Vision and Pattern Recognition*, pages 12932–12942, 2022. [2](#), [3](#)
- [49] Barbara Roessle, Jonathan T Barron, Ben Mildenhall, Pratul P Srinivasan, and Matthias Nießner. Dense depth priors for neural radiance fields from sparse input views. In *Proceedings of the IEEE/CVF Conference on Computer Vision and Pattern Recognition*, pages 12892–12901, 2022. [1](#), [2](#), [3](#)
- [50] Paul-Edouard Sarlin, Cesar Cadena, Roland Siegwart, and Marcin Dymczyk. From coarse to fine: Robust hierarchical localization at large scale. In *Proceedings of the IEEE/CVF conference on computer vision and pattern recognition*, pages 12716–12725, 2019. [1](#), [2](#)
- [51] Johannes L Schönberger and Jan-Michael Frahm. Structure-from-motion revisited. In *Proceedings of the IEEE Conference on Computer Vision and Pattern Recognition*, pages 4104–4113, 2016. [2](#)
- [52] Ken Shoemake. Animating rotation with quaternion curves. In *Proceedings of the 12th Annual Conference on Computer Graphics and Interactive Techniques*, pages 245–254, 1985. [4](#)
- [53] Vincent Sitzmann, Michael Zollhöfer, and Gordon Wetzstein. Scene Representation Networks: Continuous 3d-structure-aware neural scene representations. *Advances in Neural Information Processing Systems*, 32, 2019. [2](#)
- [54] Cheng Sun, Min Sun, and Hwann-Tzong Chen. Direct voxel grid optimization: Super-fast convergence for radiance fields reconstruction. In *Proceedings of the IEEE/CVF Conference on Computer Vision and Pattern Recognition*, pages 5459–5469, 2022. [2](#)
- [55] Matthew Tancik, Vincent Casser, Xinchun Yan, Sabeek Pradhan, Ben Mildenhall, Pratul P Srinivasan, Jonathan T Barron, and Henrik Kretschmar. Block-nerf: Scalable large scene neural view synthesis. In *Proceedings of the IEEE/CVF Conference on Computer Vision and Pattern Recognition*, pages 8248–8258, 2022. [2](#)
- [56] Matthew Tancik, Ethan Weber, Evonne Ng, Ruilong Li, Brent Yi, Terrance Wang, Alexander Kristoffersen, Jake Austin, Kamyar Salahi, Abhik Ahuja, et al. Nerfstudio: A modular framework for neural radiance field development. In *ACM SIGGRAPH 2023 Conference Proceedings*, pages 1–12, 2023. [6](#), [1](#)
- [57] Fabio Tosi, Alessio Tonioni, Daniele De Gregorio, and Matteo Poggi. Nerf-supervised deep stereo. In *Proceedings of the IEEE/CVF Conference on Computer Vision and Pattern Recognition*, pages 855–866, 2023. [3](#)
- [58] Prune Truong, Marie-Julie Rakotosaona, Fabian Manhardt, and Federico Tombari. SPARF: Neural radiance fields from sparse and noisy poses. In *Proceedings of the IEEE/CVF Conference on Computer Vision and Pattern Recognition*, pages 4190–4200, 2023. [1](#), [2](#), [3](#), [4](#)
- [59] Haithem Turki, Michael Zollhöfer, Christian Richardt, and Deva Ramanan. PyNeRF: Pyramidal neural radiance fields. *Advances in Neural Information Processing Systems*, 36, 2024. [2](#), [6](#), [7](#), [8](#), [1](#), [3](#), [5](#)
- [60] Zhou Wang, Alan C Bovik, Hamid R Sheikh, and Eero P Simoncelli. Image quality assessment: From error visibility to structural similarity. *IEEE Transactions on Image Processing*, 13(4):600–612, 2004. [5](#)
- [61] Yiheng Xie, Towaki Takikawa, Shunsuke Saito, Or Litany, Shiqin Yan, Numair Khan, Federico Tombari, James Tompkin, Vincent Sitzmann, and Srinath Sridhar. Neural fields in visual computing and beyond. In *Computer Graphics Forum*, pages 641–676. Wiley, 2022. [2](#)
- [62] Alex Yu, Vickie Ye, Matthew Tancik, and Angjoo Kanazawa. pixelNeRF: Neural radiance fields from one or few images. In *Proceedings of the IEEE/CVF Conference on Computer Vision and Pattern Recognition*, pages 4578–4587, 2021. [2](#), [3](#)
- [63] Richard Zhang, Phillip Isola, Alexei A Efros, Eli Shechtman, and Oliver Wang. The unreasonable effectiveness of deep features as a perceptual metric. In *Proceedings of the IEEE Conference on Computer Vision and Pattern Recognition*, pages 586–595, 2018. [5](#)
- [64] Tinghui Zhou, Shubham Tulsiani, Weilun Sun, Jitendra Malik, and Alexei A Efros. View synthesis by appearance flow. In *Proceedings of the European Conference on Computer Vision*, pages 286–301. Springer, 2016. [2](#)
- [65] Yin Zhou and Oncel Tuzel. VoxelNet: End-to-end learning for point cloud based 3D object detection. In *Proceedings of the IEEE Conference on Computer Vision and Pattern Recognition*, pages 4490–4499, 2018. [2](#)
- [66] Zehao Zhu, Zhiwen Fan, Yifan Jiang, and Zhangyang Wang. Fsgs: Real-time few-shot view synthesis using gaussian splatting. *arXiv preprint arXiv:2312.00451*, 2023. [1](#), [2](#)